THE JOURNAL OF BIOLOGICAL CHEMISTRY VOL. 286, NO. 16, pp. 14215–14225, April 22, 2011

Disease-associated GPR56 Mutations Cause Bilateral Frontoparietal Polymicrogyria via Multiple Mechanisms*[S]

Received for publication, September 10, 2010, and in revised form, January 25, 2011 Published, JBC Papers in Press, February 24, 2011, DOI 10.1074/jbc.M110.183830

Nien-Yi Chiang[‡], Cheng-Chih Hsiao[§], Yi-Shu Huang[‡], Hsin-Yi Chen[§], I-Ju Hsieh[‡], Gin-Wen Chang[§], and Hsi-Hsien Lin[§1]

From the [‡]Graduate Institute of Biomedical Sciences and the [§]Department of Microbiology and Immunology, College of Medicine, Chang Gung University, 259 Wen-Hwa 1st Road, Kwei-Shan, Tao-Yuan, Taiwan

Loss-of-function mutations in the gene encoding G protein-coupled receptor 56 (GPR56) lead to bilateral frontoparietal polymicrogyria (BFPP), an autosomal recessive disorder affecting brain development. The GPR56 receptor is a member of the adhesion-GPCR family characterized by the chimeric composition of a long ectodomain (ECD), a GPCR proteolysis site (GPS), and a seven-pass transmembrane (7TM) moiety. Interestingly, all identified BFPP-associated missense mutations are located within the extracellular region of GPR56 including the ECD, GPS, and the extracellular loops of 7TM. In the present study, a detailed molecular and functional analysis of the wild-type GPR56 and BFPP-associated point mutants shows that individual GPR56 mutants most likely cause BFPP via different combination of multiple mechanisms. These include reduced surface receptor expression, loss of GPS proteolysis, reduced receptor shedding, inability to interact with a novel protein ligand, and differential distribution of the 7TM moiety in lipid rafts. These results provide novel insights into the cellular functions of GPR56 receptor and reveal molecular mechanisms whereby GPR56 mutations induce BFPP.

Representing the largest group of cell surface proteins in the human proteome, G protein-coupled receptors (GPCRs)[2] play a crucial role in many biological processes, including embryonic development, central nervous system (CNS), immune system, and tumorigenesis (1–5).

One GPCR of interest known to be involved in diverse biological systems is GPR56. Also named TM7XN1, GPR56 was initially identified in melanoma cells as a novel receptor whose expression level correlated inversely to the metastatic potential of cells (6, 7). Later, it was shown to be overexpressed in human gliomas, many other tumor cell lines and cancerous tissues (8). Recently, GPR56 was found to be expressed in a subset of cytotoxic NK cells (9). In CNS, GPR56 is essential for the normal development of cerebral cortex and proper cerebellar morphogenesis (10, 11). Specifically, loss-of-function GPR56 mutations were identified as the sole cause of bilateral frontoparietal polymicrogyria (BFPP), a rare hereditary congenital disorder in human (12). Characterized by numerous small gyri on the surface of frontal cortex, BFPP patients suffer from mental retardation, motor development delay, seizures and language impairment. BFPP-associated GPR56 mutations include splicing mutations, a frameshift mutation, and several missense mutations. All but one missense mutations show essentially identical clinical syndromes, suggesting that all are null phenotypes (12–14).

GPR56 belongs to the adhesion-GPCR family characterized by the chimeric composition of a long ectodomain (ECD) and a seven-pass transmembrane (7TM) moiety (15, 16). By homology, the 7TM "GPCR" moiety is believed to be responsible for signaling. The ECD, usually consisting of multiple protein motifs implicated in protein-protein interaction and many potential glycosylation sites, is thought to mediate the "adhesion" function (16). In addition, adhesion-GPCRs are usually modified by a self-catalytic reaction at the GPCR proteolysis site (GPS) (16, 17). GPS auto-proteolysis split the adhesion-GPCR into an adhesion-ECD and a signaling-7TM subunit that associated non-covalently on the cell surface. GPS proteolysis takes place in the ER and is essential for the subcellular trafficking and function of some adhesion-GPCRs (17, 18).

Intriguingly, all BFPP-associated missense mutations identified to date are located at the extracellular region of GPR56; 4 at the N-terminal tip (R38Q, R38W, Y88C, C91S), 2 at the GPS motif (C346S, W349S), and 2 at the extracellular loops of the 7TM subunit (R565W, L640R) (12, 19). Recent studies have revealed many characteristics of GPR56; biochemical analysis showed that BFPP mutations affect predominantly protein trafficking and hence surface expression of the receptor (19). Mouse tissue transglutaminse (TG2) was identified as a GPR56 binding partner that inhibited metastasis of A375 melanoma cell *in vivo* (20). The presence of another potentially distinct cellular ligand in the pial basement membrane (BM) of cerebral cortex was recently documented (11). Experiments using *Gpr56* knock-out mice further indicated that GPR56 plays a role in the adhesion of granule cells to the extracellular matrix molecules (ECM) of BM (10). Finally, a role for GPR56 in reg-

* This study was supported by Grants from National Science Council, Taiwan (NSC96-2628-B-182-030-MY2 and NSC98-2320-B-182-028-MY3) and Chang Gung Memorial Hospital (CMRPD170013 and CMRPD160383) (to H.-H. L.).

[S] The on-line version of this article (available at http://www.jbc.org) contains supplemental Figs. S1–S7 and Tables S1 and S2.

[1] To whom correspondence should be addressed: 259 Wen-Hwa 1st Road, Kwei-San, Tao-Yuan, Taiwan. Tel.: 886-3-2118800-3321; Fax: 886-3-2118469; Email: hhlin@mail.cgu.edu.tw.

[2] The abbreviations used are: GPCR, G protein-coupled receptor; 7TM, seven transmembrane; Ab, antibody; ADAM, a disintegrin and metalloproteinase; BFPP, bilateral frontoparietal polymicrogyria; BM, basement membrane; CNS, central nervous system; CS, chondroitin sulfate; ECD, ectodomain; ECM, extracellular matrix; EGF, epidermal growth factor; Endo H, endoglycosidase H; ER, endoplasmic reticulum; GAGs, glycosaminoglycans; Fc, fragment crystallizable; GPR56, G-protein-coupled receptor 56; GPS, GPCR proteolysis site; HA, hyaluronic acid; HS, heparan sulfate; MMPs, matrix metalloproteinases; PNGase F, peptide *N*-glycosidase F; TG2, tissue transglutaminse; WT, wild-type; FACS, fluorescence-activated cell sorting.

ulating the migration of neural progenitor cell via a $G\alpha_{12/13}$ and Rho pathway was identified recently (21).

Despite these advances, much remains to be learnt regarding the molecular properties of GPR56 receptor. Through the analysis of the wild type (WT) and the BFPP-associated GPR56 point mutants, we identify herein functional characteristics of GPR56 that might provide a molecular explanation for the disorder: 1) stringent requirement for efficient cell surface expression; 2) GPS cleavage-independent shedding of GPR56; 3) Identification of a novel protein ligand that does not interact with the N-terminal BFPP mutants; 4) GPR56-ligand interaction promotes cell adhesion; 5) Localization of the 7TM subunit to membrane lipid rafts. In conclusion, we suggest the null phenotype displayed by the different BFPP-associated mutations results from multiple mechanisms.

EXPERIMENTAL PROCEDURES

Reagents and Antibodies—General reagents were obtained from Sigma-Aldrich, unless otherwise specified. Oligonucleotide primers were supplied by Tri-I Biotech (Taipei, Taiwan). DNA and protein reagents were obtained from Invitrogen (Carlsbad, CA), Qiagen (Valencia, CA), Fermentas (ON, Canada), New England Biolabs, and Amersham Biosciences (GE Healthcare). Antibodies (Abs) used in the study are: anti-HA (clone 16B12) from Covance; clone HA-7 from Sigma; anti-HA-FITC from MACS (Bergisch Gladbach, Germany). Anti-Myc was from Invitrogen. FITC-conjugated Goat anti-mouse IgG was from Jackson ImmunoResearch (West Grove, PA). Mouse IgG_1 isotype control (clone 11711) was from R&D Systems. Anti-actin (clone C4) was from Chemicon. Anti-Vinculin (1:400; clone hVIN-1) and anti-paxillin (1:500; clone PXC-10) were from Sigma. Anti-human IL-8 (1:250) and recombinant human IL-8 (CXCL8) were from PeproTech (Rocky Hill, NJ). Anti-transglutaminase II (1:200; clone CUB 7402) was from Thermo Scientific (Fremont, CA). Recombinant human epidermal growth factor (HuEGF; 0.1 μg/ml) was from Invitrogen. Anti-caveolin-1 (clone 7C8) was from Upstate (Lake Placid, NY), anti-transferrin receptor (CD71) (1:500; clone H68.4) was from Zymed Laboratories Inc. (San Francisco, CA).

Cell Culture—All cell culture media and supplements, including fetal calf serum (FCS), L-glutamine, penicillin, and streptomycin were purchased from Invitrogen. All cell lines used in this study were purchased from the American Type Culture Collection (Manassas, VA) and cultured in conditions as suggested.

Construction of Expression Vectors and Cell Transfection—For vector construction, full-length cDNA fragments were amplified by PCR using the human GPR56 cDNA clone (TrueClone™, NM_005682.4, OriGene Technologies), human TG2 (ATCC® No:7502536) and mouse TG2 (ATCC® No:MGC-1193) as templates. Standard molecular biology techniques were used to engineer expression constructs for various mutant and recombinant GPR56 fusion proteins using specific primer sets (supplemental Table S1). GPR56 site-directed mutants were generated in a two-step PCR procedure as described previously using primer pairs listed in supplemental Table S2. For the construction of GPR56-mouse fragment crystallizable (mFc) expression vectors, a cDNA fragment encoding the entire extracellular domain of GPR56 was subcloned into pSecTaq-mFc as described previously. All expression constructs were sequenced to confirm their sequence fidelity. Cells were transfected with purified plasmid DNA using Lipofectamine™ (Invitrogen) as described previously (22).

Immunoblotting Analysis—Cells were lysed in RIPA lysis buffer (20 mM Tris-HCl pH7.4, 5 mM $MgCl_2$, 100 mM NaCl, 0.5% Nonidet P-40, and 1× Complete Protease Inhibitors) supplemented with 1 mM sodium orthovanadate, 1 mM AEBSF, and 5 mM Levamisole. Proteins were quantified using the Bicinchoninic acid (BCA) protein assay kit (Pierce). For de-glycosylation experiments, protein samples were first denatured in denaturing buffer (0.5% SDS, 1% β-mercaptoethanol) at 85 °C for 3 min. Denatured samples were incubated with either endoglycosidase H (1 unit) alone or different combinations of PNGase F (1 unit), *O*-glycosidase (0.5 mU), and neuraminidase (1.0 mU) in 20 mM sodium phosphate buffer, pH 6.8 at room temperatures for 1–4 h, then at 37 °C overnight, prior to SDS-PAGE and Western blot analysis, which were carried out using standard procedures as described previously (22, 23).

For far-Western immunoblotting, proteins were separated and transferred to PVDF membranes. Membranes were then soaked in blocking buffer (PBS containing 5% nonfat skimmed milk and 0.1% Tween-20) for 1 h at 4 °C. Blots were then incubated with GPR56-mFc (1 μg/ml) diluted in blocking buffer for 1 h at 4 °C, followed by extensive washes in washing buffer (0.1% Tween 20/PBS). The binding of GPR56-mFc was revealed with ECL substrate (Pierce) after the membranes were incubated with horseradish peroxidase (HRP)-conjugated goat anti-mouse Fc Ab (1:5000) in blocking buffer.

Flow Cytometry and Confocal Immunofluorescent Microscopy—Transiently transfected cells, either harvested from plates or cultured on coverslips (BD BioCoat™ Poly-D-Lysine, BD Biosciences), were fixed in 4% paraformaldehyde/PBS at 4 °C for 10 min. Cells were then blocked for 1 h in cold blocking buffer (1% BSA/5% serum of 2nd Ab/PBS) with or without 0.1% saponin. Cells were subsequently incubated with the indicated primary antibody diluted in blocking buffer for 1 h before washing. Cells were then incubated for 1 h with fluorochrome-conjugated goat anti-mouse IgG in blocking buffer (1:200). Cells were washed three times in cold PBS and subjected to analysis by FACScan flow cytometer (BD Biosciences) or confocal microscopy. For subcellular localization analysis, cells were co-transfected with an ER-GFP expression construct (pCMV/Myc/ER/GFP, Invitrogen). Alexa-Fluor 647-conjugated anti-mouse IgG (1:200; Invitrogen) was used as the 2nd Ab. Coverslips were mounted onto slides with anti-fade mounting medium (ProLong® Gold Antifade reagent with DAPI, Invitrogen). Fluorescence images were taken at 1000-fold magnification (Zeiss LSM 510 META). For confocal observation of cell morphology, proteins of interest were coated onto 12 mm coverslips in the 24 well-plate. Following thorough wash and blocking (2% BSA in HBSS) at 37 °C for 1 h, single cell suspension ($\sim 5 \times 10^5$ cell/ml) was added to each well and incubated at 37 °C for 3 h. Cells were then fixed with 4% paraformaldehyde and processed for immunostaining using indicated Abs. Cells were finally stained with phalloidin (10 μg/ml) for 1 h. The coverslips were removed and cov-

ered on DAPI drops (10 μl each) on slides for microscopic observation (Zeiss LSM 510 META).

Purification of GPR56-mFc Fusion Protein and Cellular Ligand Binding Assays—Soluble GPR56-mFc fusion proteins were produced and purified as described previously (24, 25). The purified fusion proteins were dialyzed in 50 mM Tris buffer, pH 7.4 for 24 h at 4 °C, and stored at −80 °C.

To search for the cell lines expressing putative GPR56-ligand, two well-described methods were employed (24, 25). Briefly, cells of interest were harvested and suspended in 0.1% BSA/PBS at 1×10^6 cells/ml. For the Dynabead-cell binding assay, 25 μl of protein A or G-conjugated paramagnetic Dynabeads® (Dynals; Lake Success NY) were washed three times in 0.1% BSA/PBS for 5 min each. GPR56-mFc protein (5 μg/reaction) was mixed with Dynabeads for 1 h, washed to remove unbound proteins, and incubated with cells in 0.1% BSA/PBS (1×10^6 cells/ml; total volume, 0.5 ml) on ice for 1 h with constant rotation. The bead-cell complexes were washed three times in 0.1% BSA/PBS by magnetic separation. The binding ability of cells to GPR56-mFc-coated beads was assessed by cell counting or microscope observation. For the fluorescence-activated cell sorting (FACS)-based cell binding assay, a previously described method was modified (25). Briefly, cells were subjected to the standard flow cytometry analysis, but used the GPR56-mFc probe (5 μg/ml) as the primary Ab. Where indicated, cells were pretreated or treated simultaneously with various reagents in the presence of the GPR56-mFc probes. FITC-conjugated goat anti-mFc Ab was used as the 2nd Ab. Binding was analyzed by FACScan flow cytometer (BD Bioscience).

siRNA Transfection—The siRNA reagents were purchased from Dharmacon Human siGENOME® SMARTpool® (TGM2 gene; gene ID 7052) (Thermo Fisher Scientific). Briefly, HeLa cells were seed at 5×10^4 cells/ml and transfected with 0.2 μM scrambled or hTG2 siRNA, using DharmaFECT1 according to the manufacturer's protocols. Cells were analyzed 72 h post-transfection as described.

Cell Adhesion Assay—Proteins of interest were diluted in HBSS to a final concentration of 1, 5, 10, and 20 μg/ml and coated on 96 well-plate (GeneDireX®) (100 μl/well) at 4 °C overnight. Wells were then washed and blocked with 100 μl of blocking buffer (2% BSA in HBSS) at 37 °C for 1 h. Single cell suspension of HT-1080 or U87MG cells (1×10^6 cell/ml) was added to each well (100 μl/well) and incubated at 37 °C for 1.5 h. Non-adherent cells were carefully removed by thorough wash, and adherent cells were fixed with 100 μl of 1% glutaraldehyde (diluted in 0.1 M cacodylate buffer) per well for 1 h at 4 °C. The glutaraldehyde-fixed cells were stained with 100 μl of 1% methylene blue in 0.01 M borate buffer for 30 min at room temperature. The excess dye was washed by ddH_2O, and 100 μl of ethanol was added to each well. The dye dissolved in ethanol was transferred to another new 96 well-plate for A_{595} measurement.

Lipid Raft Separation—All procedures are carried out on ice. Cells ($\sim 5 \times 10^6$ cells) were washed three times with ice-cold PBS, then lysed in 150 μl ice-cold TNET buffer (25 mM Tris/HCl, pH 7.5, 150 mM NaCl, 5 mM EDTA, 1 mM EGTA, 1% Triton X-100, 10 mM NaF, 1 mM sodium pyrophosphate, 1 mM Na_3VO_4 and 1× Protease inhibitor mixture) for 30 min. Total cell lysates were passed through a 25-gauge needle 20 times on ice, and then centrifuged at 1,000 × *g* for 10 min at 4 °C to collect the supernatant for protein quantification. Typically, 200 μl of cell lysate (~500 μg protein) were mixed with 400 μl of 60% OptiPrep™ gradient medium and then placed at the bottom of a 5 ml of polyallomer ultracentrifuge tube (Beckman). Samples were overlaid sequentially with 3,400 μl of 30% and 200 μl of 5% ice-cold OptiPrep™ gradient medium diluted in TNET buffer, and subjected to ultracentrifugation (Beckman) at 200,000 × *g* for 16 h at 4 °C. Following ultracentrifugation, seven equal fractions (~600 μl/fraction) were collected from the top of the tube.

RESULTS

BFPP-associated GPR56 Mutant Proteins Are Deficient in Intracellular Trafficking, Cell Surface Expression and/or GPS Proteolytic Cleavage—To investigate the effect of BFPP-associated point mutations on the expression and GPS proteolytic modification of GPR56, WT, and mutant GPR56 proteins were tagged with a hemagglutinin (HA) and c-Myc epitope at the N and C terminus, respectively (Fig. 1*A*). As expected, WT GPR56 was found to be cleaved producing an N-terminal ECD fragment (α-subunit) and a C-terminal 7TM fragment (β-subunit) (Fig. 1*B*). The α-subunit as detected by anti-HA as well as a GPR56-specific mAb (CG3, manuscript in preparation) shows a broad and smearing pattern at ~60–70 kDa, suggesting potential glycan decoration as predicted by the many *N*- and *O*-link glycosylation sites in GPR56 (supplemental Fig. S1*A*). In contrast, anti-Myc Ab detected three predominant bands of ~25 kDa, ~50 kDa, and ~75 kDa (Fig. 1*B*), which are detected in different methods of sample preparation (supplemental Fig. S1*B*) and hence believed to be the monomeric and SDS-resistant dimeric and trimeric β-subunits, respectively.

In cells expressing GPR56-R38W, -Y88C, -C91S, -R565W, or -L640R, both α- and β-subunits were also detected independently, albeit with a smaller α-subunit and of less abundance (Fig. 1*B*). Thus, GPS auto-proteolysis is not affected by these mutations. Of note is the much weaker expression of R565W β-subunit comparing to other mutants. Moreover, we found that the β-subunit tends to aggregate at the top of the gel in addition to forming oligomers. Intriguingly, the aggregation is much more apparent in R565W, L640R, C346S, and W349S mutants (Fig. 1*B*). In cells expressing C346S or W349S mutant, a single weak band of approximately ~75 kDa representing the uncleaved full-length receptor is detected. Thus, C346S and W349S mutations not only reduced the expression level, but also abolished GPS proteolysis (Fig. 1*B*). Taken together, these results indicate that the expression level and protein modification (glycosylation and/or GPS proteolysis) were affected in these mutants.

The reduced expression levels of GPR56 mutants were subsequently confirmed by flow cytometry analysis (Fig. 1*C*). Interestingly, for each mutant the surface expression, but not the total expression level was markedly reduced when compared with that of WT receptor (Fig. 1*C*). These results confirm previous conclusions (19) and strongly indicate that all BFPP point mutations impaired the subcellular trafficking of GPR56 receptor to some extent, reducing its cell surface expression.

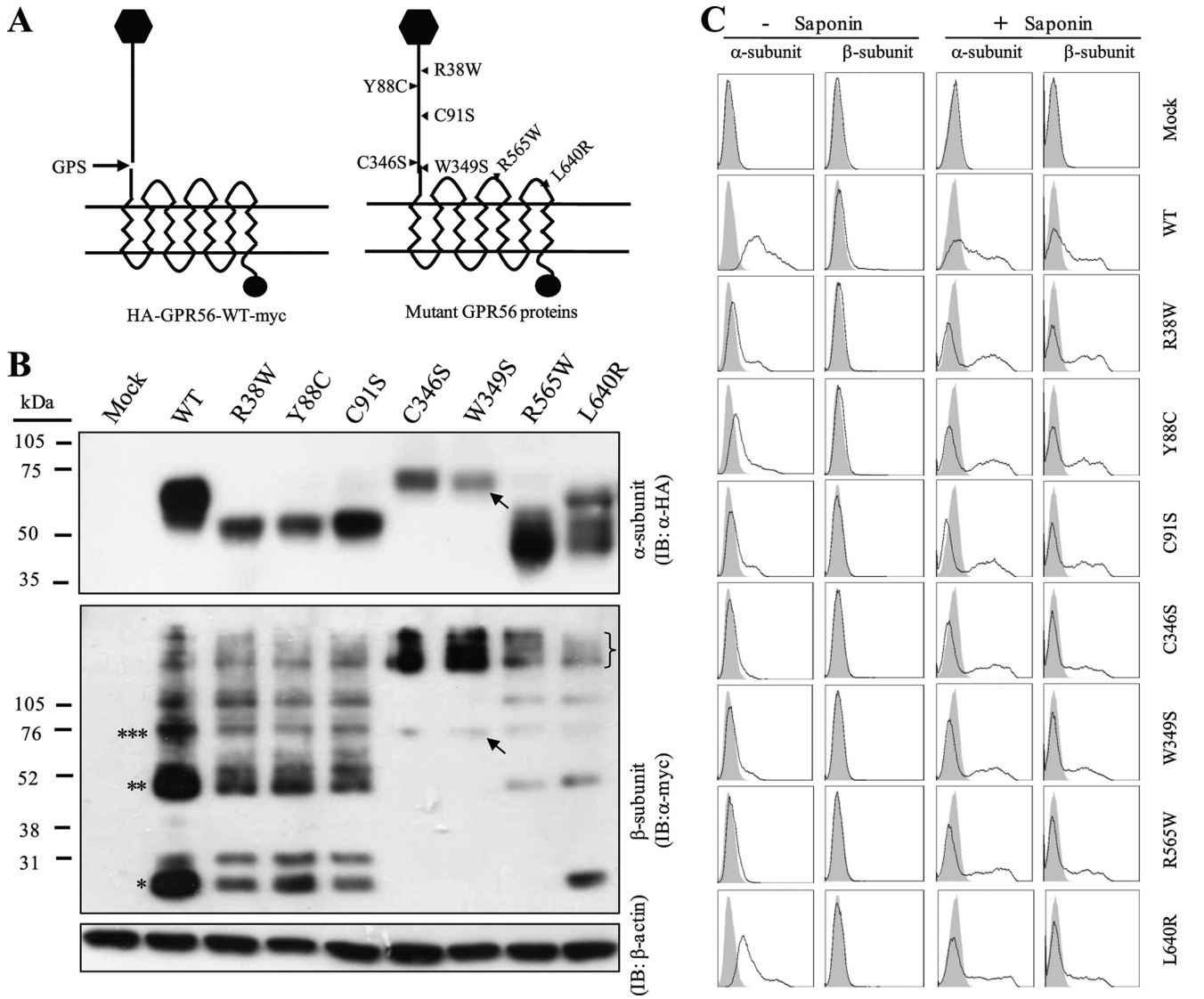

FIGURE 1. **Biochemical analysis of GPS autoproteolysis and expression of GPR56 receptor and its various mutants.** *A*, schematic representation of the WT GPR56 and the BFPP-associated mutants. GPR56 was tagged with the HA- (*black hexagon*) and Myc-epitope (*black circle*) at the N and C terminus, respectively. The *arrow* indicates the conserved GPS site. *B*, Western blot analysis of total cell lysates from HEK293T cells expressing GPR56-WT or mutants as indicated. Blots were probed with anti-HA (*upper panel*) and anti-Myc (*lower panel*) to detect the α-subunit and β-subunit, respectively. The monomeric, dimeric, and trimeric forms of β-subunit were indicated by 1, 2, and 3 *asterisks*, respectively. The *arrow* denotes the uncleaved single-chain C346S and W349S mutants. The *curly bracket* indicates β-subunit aggregates. *C*, flow cytometry analysis of cell surface (without saponin) and intracellular expression (with saponin) of GPR56 receptors as indicated using anti-HA (α-subunit) or anti-Myc (β-subunit) antibodies. The *gray area* represents the isotype control.

GPR56 Mutants Are Structurally Unstable and Retained Mostly in the ER—We next investigated the subcellular localization of WT and mutant GPR56 proteins. Confocal immunofluorescence staining revealed a strong surface expression of WT-GPR56, but weak surface expression of R38W, R565W, and L640R mutants. No cell surface signals were ever detected for the C346S protein (Fig. 2*A*). On the other hand, strong intracellular signals were seen in cells expressing R38W, C346S, R565W, and L640R mutants. Most importantly, these intracellular signals were found to co-localize with the ER marker, suggesting that these mutant proteins were retained mostly in ER (Fig. 2*A*).

The retention of mutant GPR56 in ER was further confirmed by EndoH digestion, which is highly specific for the *N*-linked high mannose-type glycans found in ER-lumen glycoproteins. Fig. 2*B* shows that WT GPR56 is EndoH-resistant whereas the R38W, C346S, and R565W mutants are EndoH-sensitive, confirming the mutants are indeed mostly trapped within ER. Next, we examined the extent of GPR56 glycosylation. A slight reduction in sizes (~2–3 kDa) was observed for the WT α-subunit by neuraminidase treatment, suggesting the presence of sialic acids. In contrast, a dramatic molecular mass change (~60–70 kDa to ~40 kDa) was seen in the same samples treated with PNGase F alone or PNGase plus O-glycosidase (Fig. 2*C*). As the predicted molecular mass of unmodified α-subunit is ~40 kDa, this indicated that the extracellular domain of WT GPR56 is indeed heavily glycosylated. In addition, as there is no apparent size difference between samples treated with PNGase alone and PNGase plus *O*-glycosidase, the glycans decorated on GPR56 are believed to be mostly on *N*-glycosylation sites and are apparently modified with sialic acids.

Analysis of R38W and R565W mutants revealed a similar molecular mass shift by PNGase F and PNGase plus *O*-glycosi-

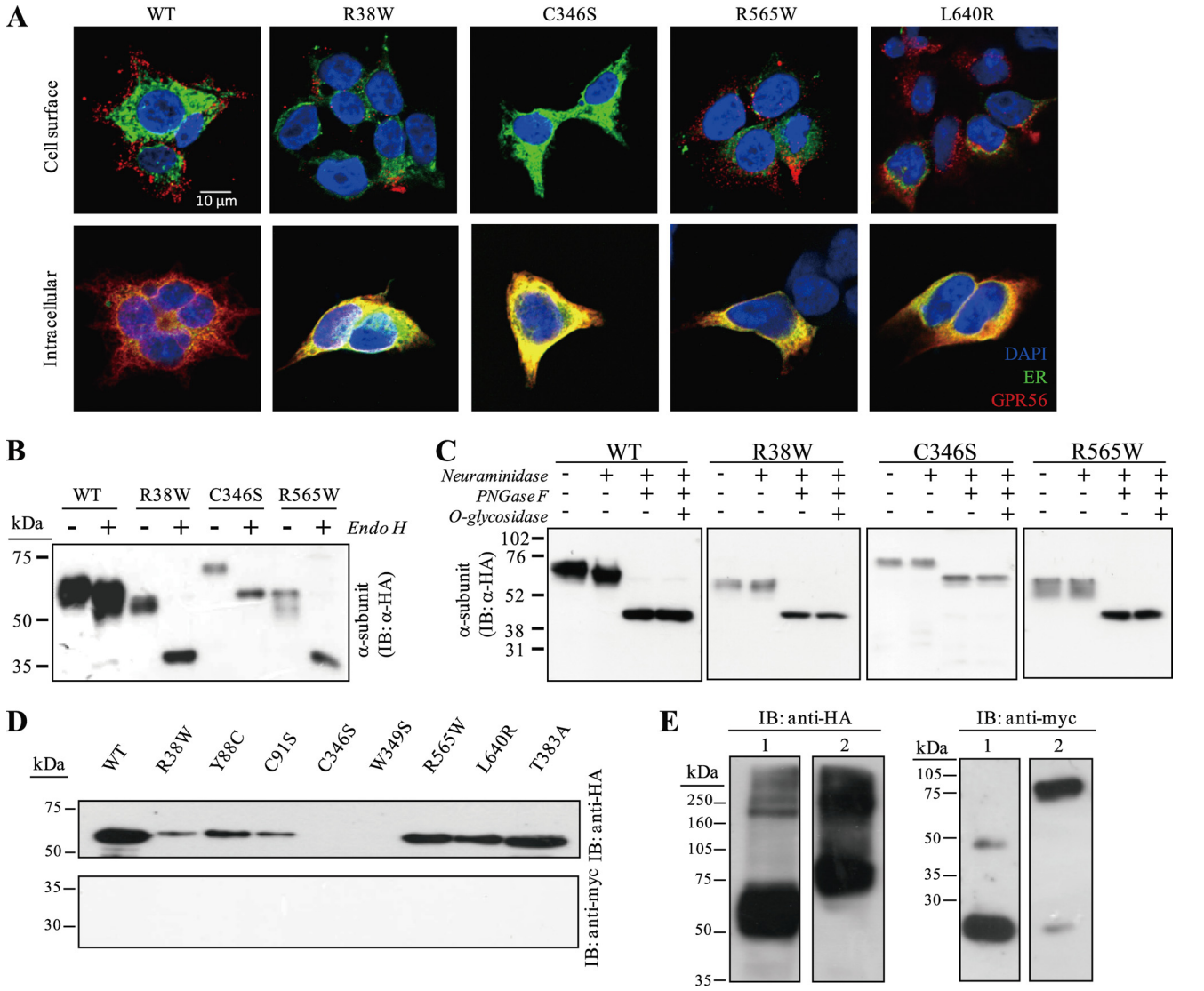

FIGURE 2. **Expressional characteristics of GPR56 and BFPP-associated mutants.** *A*, cell surface and intracellular subcellular localization of the wild-type GPR56 and its various mutants was analyzed by confocal immunofluorescence staining using anti-HA Ab (α-subunit; *red*). ER was marked by green fluorescence due to co-transfected pCMV/myc/ER/GFP, while nucleus was stained with DAPI (*blue*). *B* and *C*, endo H digestion and deglycosylation of GPR56 proteins. Total cell lysates of HEK293T cells transfected with various GPR56 receptors were treated with or without Endo H (*B*) and various glycosidases (*C*) as indicated, followed by Western blot analysis. *D*, shedding of GPR56. Western blot analysis of conditioned media from HEK293T cells transfected with WT and mutant GPR56 receptors. *E*, Western blot analysis of total cell lysate of cells expressing GPR56-WT (*lane 1*) and GPR56-T383A-myc (*lane 2*) using anti-HA (*left panel*) and anti-myc (*right panel*) for the α-subunit and the β-subunit, respectively.

dase treatment, producing a band of ~40 kDa. Likewise, a shift from ~75 kDa to ~60 kDa was observed for the C346S mutant under the same condition (Fig. 2*C*). Interestingly, the mutants did not show a similar size reduction after neuraminidase treatment. As the addition of sialic acids normally takes place in the Golgi apparatus, this indicated again that the majority of GPR56 mutants do not exit from the ER. This is consistent with the fact that a smaller α-subunit was detected in GPR56 mutants (Fig. 1*B*). Altogether, consistent with the previous report (19), WT GPR56 is a heavily glycosylated cell surface protein, while the BFPP mutants are mostly ER-resident proteins decorated with *N*-linked high mannose-type glycans.

The ER localization and the reduced expression level of GPR56 mutants suggested that they might not be folded properly and hence are prone to degradation. Indeed, the expression of GPR56 mutants and to a less extent the WT protein was enhanced greatly in cells treated with the proteasome inhibitor, MG132, suggesting that the BFPP-associated mutations lead to misfolding and degradation of GPR56 (supplemental Fig. S2).

Shedding of GPR56 Extracellular Domain—Previous studies have identified soluble GPR56 α-subunit in conditioned media, suggesting active shedding of GPR56 protein (19). Western blot analysis showed that GPR56 α-subunit was indeed readily detected in media collected from cells expressing WT GPR56 as well as the R38W, Y88C, C91S, R565W, and L640R mutants (Fig. 2*D*). On the contrary, no soluble α-subunit from cells expressing C346S and W349S mutants was detected. The amount of soluble α-subunit correlated positively with the surface levels of respective receptors. Importantly, no β-subunit was ever detected in all samples examined, indicating that the α-subunit is indeed the result of receptor shedding and not of cell death.

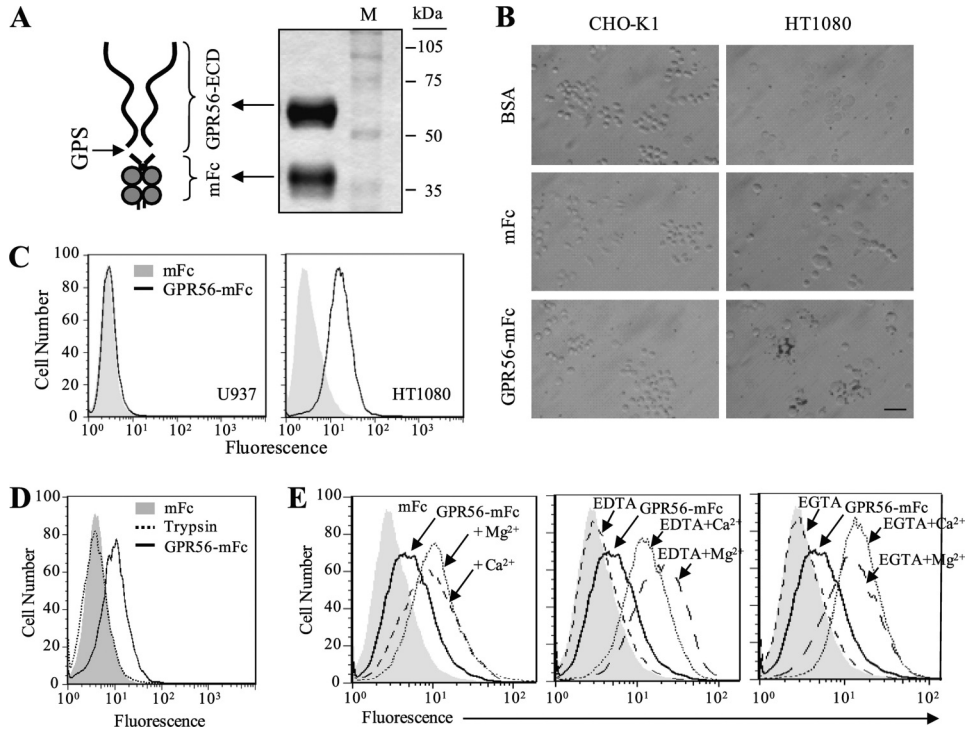

FIGURE 3. **Identification and characterization of a putative cellular ligand of GPR56.** *A*, *left panel*, schematic representation of the GPR56-mFc fusion protein probe for ligand search. The GPR56 ECD and the mFc fragment are shown as a *wavy line* and *two circles*, respectively. The GPS cleavage site is indicated by an *arrow*. *Right panel*, Coomassie Brilliant Blue staining of purified GPR56-mFc. *B*, dynabead cell-binding assay. Dynabeads coated with BSA control, mFc only, or GPR56-mFc protein were incubated with CHO-K1 (ligand-negative) or HT1080 (ligand-positive) cells. Following extensive washes, cell-dynabead complexes were observed with microscope. Scale bar, 50 μm. *C*, FACS-based cell binding assay. HT1080 and U937 represent ligand-positive and ligand-negative cells, respectively. mFc proteins were used as a negative control. *D*, putative cellular ligand is a trypsin-sensitive surface protein. HT1080 cells were treated with or without 10 μg/ml trypsin for 10min at 37 °C before performing the ligand binding assay. *E*, GPR56-ligand interaction is divalent cation-dependent. The cellular ligand binding assay was carried out in the presence of EDTA or EGTA with or without exogenous divalent cations as indicated.

The shedding of α-subunit could be due to the dissociation of cleaved ECD subunit from plasma membrane or other unspecified active processes. To investigate whether GPS proteolysis is essential for GPR56 shedding, GPR56-T383A mutant was analyzed. The T383A substitution disrupts the conserved GPS cleavage site and hence is expected to be a cleavage-deficient mutant. This is clearly demonstrated by the detection of a major single band of ~80 kDa by both anti-HA and anti-Myc Abs (Fig. 2*E* and supplemental Fig. S3*A*). Surprisingly, soluble α-subunit was still detected in conditioned medium of T383A mutant-expressing cells at a comparable level to that of WT protein-expressing cells (Fig. 2*D*). This data strongly suggests that shedding of α-subunit is mediated by a second cleavage event independent of GPS proteolysis. Indeed, α-subunit shedding was greatly reduced in cells treated with GM6001 but not other protease inhibitors, suggesting the potential involvement of MMPs or ADAMs (supplemental Fig. S3*B*). Therefore, GPR56 α-subunit is present not only on the cell surface but also in the extracellular milieu. Most interestingly, some of the GPR56 mutants also shed their α-subunit despite their reduced surface expression levels and predominant ER localization.

Identification and Characterization of a Novel TG2-independent Cellular Ligand for GPR56—Being an adhesion-GPCR, it is reasonable to expect that GPR56 might interact with certain specific cellular ligands. As mentioned earlier, mouse TG2 has been identified previously as a GPR56 binding partner (20). Moreover, recent studies by Li *et al.* have shown a potentially distinct GPR56-ligand in the mouse pial BM (11). Herein we applied a well-established methodology to search for the presence of GPR56 cellular ligands (24). A chimeric protein containing the extracellular domain of GPR56 fused to a truncated mouse Fc (mFc) region was produced as a probe (Fig. 3*A*). A panel of cell lines was screened for their ability to bind GPR56-mFc using either paramagnetic beads (Fig. 3*B*) or a FACS-based cell-binding assay (Fig. 3*C*). Both assays show that many but not all cell lines specifi-

TABLE 1
Summary of cell lines screened for the expression of GPR56-ligand

Cell line	Ligand binding	% of ligand$^+$ cells
HT-1080	+++++	68.1
NIH/3T3	++++	57.6
HeLa	+++	40.4
M059K	+++	35
COS7	++	31.9
U87MG	++	23.9
C32	++	23.8
MCF-7	++	17.6
MDA –MB-231	++	15.6
HEK-293T	+	11.3
K562	+	9.9
G5T	+	9.7
A2058	+	7.2
A375	+/–	4.7
Jurkat	+/–	4.6
CHO-K1	+/–	4.1
MeWo	+/–	3.4
MEL	–	0.9
THP-1	–	0.6
CHO-618	–	0.5
CHO-677	–	0.2
U937	–	0.1

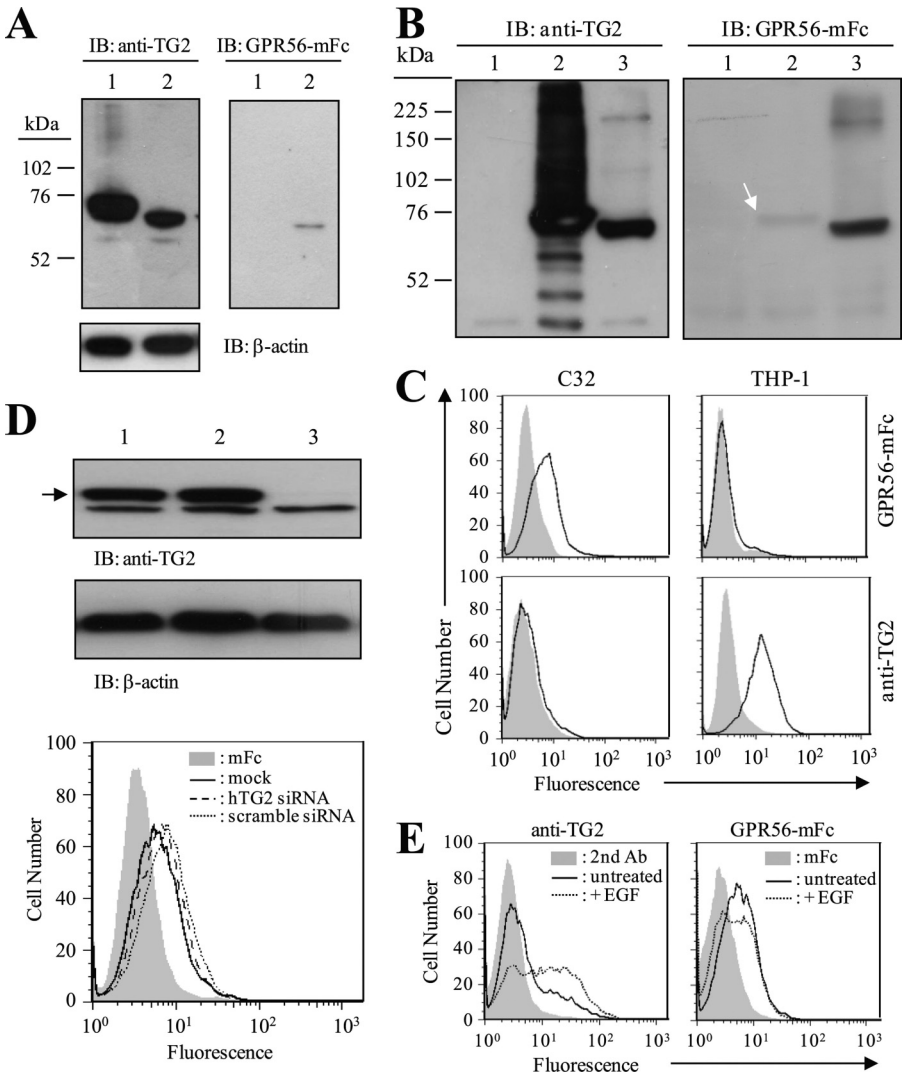

FIGURE 4. **TG2 is not the putative GPR56 ligand.** *A*, far Western blot analysis of GPR56 binding to endogenous TG2. TG2 expression was shown in HT1080 cells (*lane 1*) and NIH3T3 cells (*lane 2*) using anti-TG2 Ab (*left panel*) or GPR56-mFc (*right panel*) as probes. Anti β-actin was used to confirm equal loading of cell lysates. *B*, far Western blot analysis of GPR56 binding to exogenous TG2. HEK293T cells were transiently transfected with mock (*lane 1*), Myc-tagged human TG2 (*lane 2*) or mouse TG2 (*lane 3*) expression constructs. TG2 expression was shown using anti-TG2 Ab (*left panel*) or GPR56-mFc (*right panel*) as probes. *C*, flow cytometry analysis of surface TG2 and GPR56-ligand expression in C32 and THP-1 cells. *D* and *E*, manipulation of TG2 expression in HeLa cells does not change the expression of the putative GPR56 ligand. TG2 expression in HeLa cells was knock-down by siRNA (*D*) or up-regulated by EGF (0.1 μg/ml) (*E*) and analyzed for GPR56-ligand binding ability. *D*, *top panel*, Western blot analysis of TG2 expression in cells transfected with mock (*lane 1*), scramble siRNA (*lane 2*), and human TG2 siRNA (*lane 3*). *Bottom panel*, FACS-based cell-binding assay of GPR56 binding to the putative cellular ligand. *E*, flow cytometry analysis of the expression of surface TG2 (*left panel*) and GPR56 ligand (*right panel*) in cells treated with or without EGF.

cally interact with GPR56-mFc, suggesting the presence of a putative ligand for GPR56 (Fig. 3, *B* and *C* and Table 1).

The characteristics of the putative ligand were investigated further using HT-1080 cells, a strong ligand-expressing cell line. First, we found that trypsin treatment completely abolished GPR56 binding, indicating the ligand is a cell surface protein (Fig. 3*D*). Next, we demonstrated the GPR56-ligand interaction is divalent cation-dependent because the binding was completely inhibited by EDTA and EGTA, but was restored by the addition of calcium and magnesium (Fig. 3*E*).

The identification of mouse TG2 as an ECM ligand of GPR56 prompted us to investigate whether human TG2 is the putative GPR56 ligand identified here. Our preliminary data showed that TG2 is ubiquitously expressed in all cell lines tested, including ligand-negative cells (supplemental Fig. S4*A*). Moreover, the expression levels of surface TG2 on ligand-positive cells do not correlate with the expression profile of GPR56-ligand (supplemental Fig. S4*B*). These results imply that human TG2 is unlikely the putative GPR56-ligand. To confirm this, binding of GPR56 to TG2 was analyzed by far-Western blotting. As shown in Fig. 4*A*, while GPR56-mFc binds well to mouse TG2 it fails to bind human TG2. The same results are seen in other human and mouse cell lines (supplemental Fig. S4*C*), indicating that GPR56 binding to TG2 is species-restricted.

To answer this question unambiguously, Myc epitope-tagged human and mouse TG2 were engineered and expressed. Again, GPR56-mFc was shown to bind avidly to mouse TG2, but almost none to human TG2 (Fig. 4*B*). As the GPR56-binding site of human TG2 might be distorted by SDS-PAGE treatment, additional evidence was searched to show that human TG2 is not the GPR56 ligand. To this end, we identified a human amelanotic melanoma cell line, C32, which displayed no

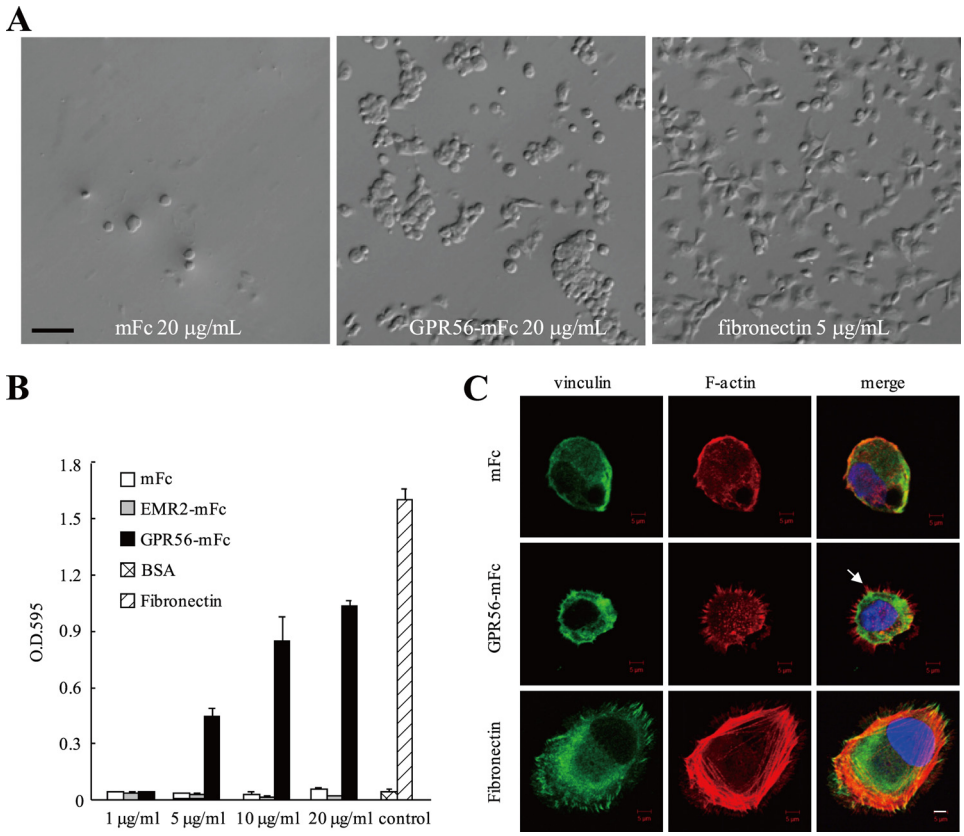

FIGURE 5. **GPR56-ligand interaction promotes cell adhesion.** *A* and *B*, cell adhesion assay showing the adhesion of HT1080 cells onto plates coated with proteins of interest as indicated (*A*) microscopy observation of cell adhesion. Scale bar, 100 μm. *B*, graph showing dose-dependent cell adhesion to GPR56-mFc. *C*, confocal microscopy showing vinculin (*green*) and actin (*red*) staining of cells adhered to fibronectin or GPR56-mFc. The *arrow* indicates the filopodia. Scale bar, 5 μm.

cell surface TG2 but bound strongly to GPR56-mFc. Conversely, THP-1 cells were found to express high levels of cell surface TG2 but showed nil GPR56-mFc binding (Fig. 4*C*). Finally, we found no changes in the ligand binding activity in HeLa cells even after its TG2 expression was reduced by siRNA knock-down or up-regulated by epidermal growth factor (Fig. 4, *D* and *E*). Thus, we conclude that human TG2 is not a cellular ligand for GPR56. Taken together, GPR56 α-subunit is capable of interacting with mouse TG2 as well as a novel TG2-independent protein ligand.

GPR56-ligand Interaction Promotes Cell Adhesion—Based on the fact that GPR56 can be partially shed into conditioned medium and that its α-subunit is able to interact with a novel cellular ligand, we asked the potential consequence of GPR56-ligand interaction using a cell adhesion assay. HT-1080 cells were allowed to incubate on 96-well plates coated with GPR56-mFc. Cell adhesion was evaluated by microscopic observation, cell fixation and staining, as well as confocal immunofluorescence staining (Fig. 5). Cells were found to adhere to GPR56-mFc in a dose and divalent cation-dependent manner at concentrations between 5–20 μg/ml (Fig. 5*B* and data not shown). The binding is specific as cells did not show any adherence to control proteins such as BSA and mFc. At 20 μg/ml, cell adhesion to GPR56 is almost as strong as to fibronectin at 5 μg/ml. However, the morphology of cells adhered onto GPR56-mFc and fibronectin is different as shown by phase contrast and confocal microscopy (Fig. 5, *A* and *C* and supplemental Fig. S5). Specifically, cells adhered on fibronectin are well-spread with the formation of typical stress-fibers and focal adhesion, whereas GPR56-adhered cells show a more rounded morphology with multiple filopodia. This result indicated that GPR56-ligand interaction can promote cell adhesion but is not strong enough to induce cell spreading and stress fiber formation.

BFPP-associated N-terminal Mutations Impair GPR56-ligand Interaction—Although BFPP-mutations severely reduced the expression levels of GPR56, some BFPP mutants can still be expressed on the cell surface and even shed into conditioned medium (Figs. 1 and 2). To investigate the binding characteristics of these mutants to the putative cellular ligand, three relevant mutant GPR56-mFc proteins (R38W, Y88C, and C91S) were produced and probed on HT-1080, NIH-3T3 and M059K cell lines (Fig. 6*A*). Flow cytometry analysis showed that both R38W and Y88C mutants lost the ligand-binding activity, while the C91S mutant reduced the ligand-binding ability (Fig. 6*A*). Similarly, cell adhesion assay showed that all three mutants fail to promote HT-1080 cell adhesion (Fig. 6*B* and supplemental Fig. S6). More importantly, ligand-positive U87MG human glioblastoma cell line was found to display a dose-dependent adhesion activity toward WT GPR56, but no reaction with the three GPR56 N-terminal mutants (Fig. 6*C*). Therefore, the three N-terminal mutations not only reduce trafficking and surface expression of GPR56, but also impair its ligand binding and hence cell adhesion activity.

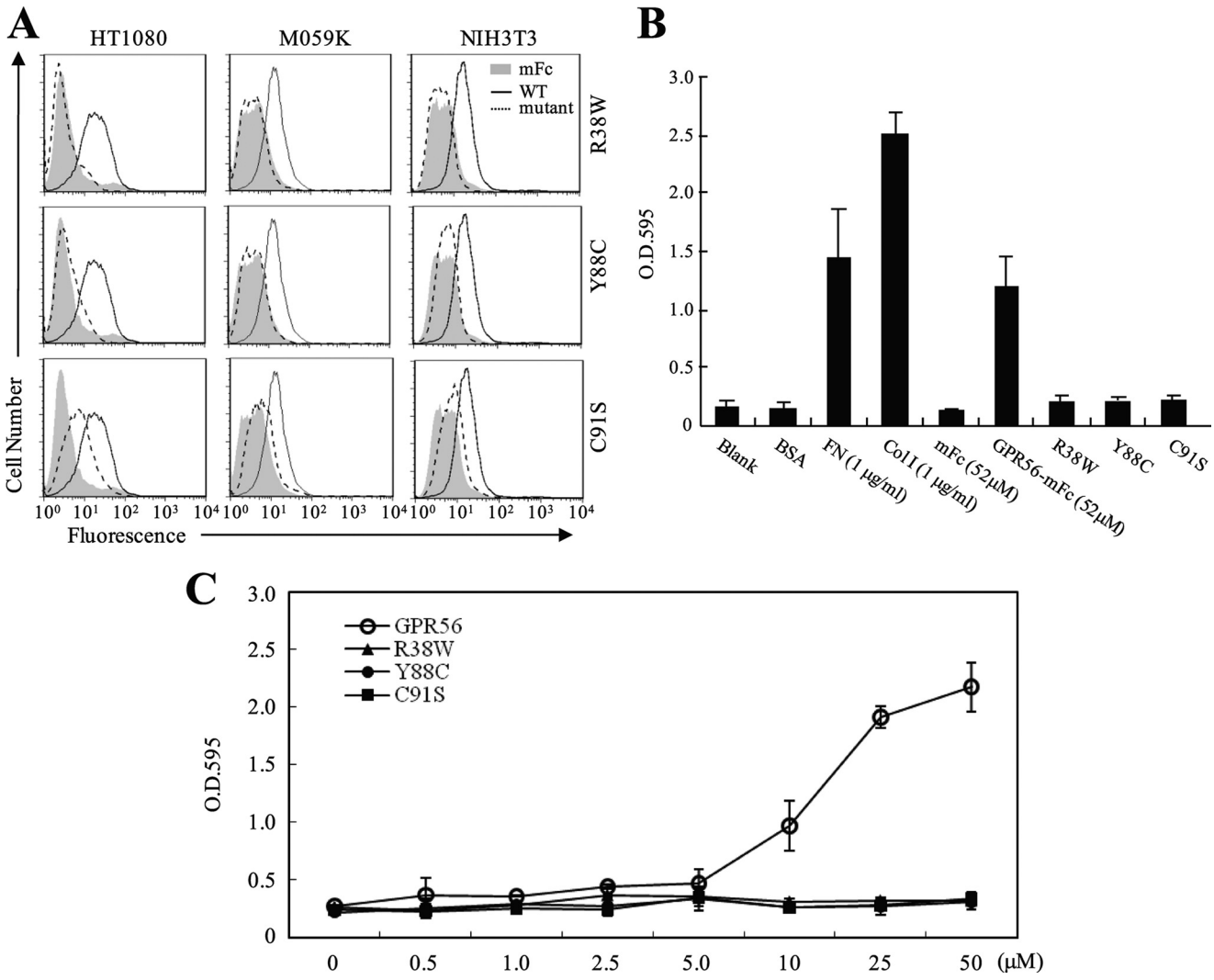

FIGURE 6. **BFPP-associated N-terminal GPR56 mutants do not interact with the putative cellular ligand.** *A*, FACS-based cell-binding assay was carried out in HT1080, M059K, and NIH3T3 cells using mFc proteins as a negative control (*gray*) and GPR56-mFc fusion protein as a positive control (*solid line*). Three N-terminal BFPP mutants (R38W, Y88C, and C91S) (*dotted line*) were analyzed for their ligand binding ability. *B*, cell adhesion assay was carried out using HT1080 cells on 96-well plates coated with control proteins and WT and mutant GPR56-mFc proteins as indicated. Data are means ± S.E. of four independent experiments performed in triplicate. *C*, adhesion of U87MG cells to 96-well plates coated with different concentrations of GPR56-mFc proteins as indicated. Data are means ± S.E. of three independent experiments performed in triplicate.

Differential Distribution of the GPR56 7TM-subunit to the Lipid Rafts—In an independent study examining the membrane distribution of the α- and β-subunits of a related adhesion-GPCR, EMR2, we have shown that the two subunits of EMR2 do not necessarily associate as a receptor complex. Specifically, we found that EMR2 α- and β-subunits localized preferentially to distinct membrane subdomains; the α-subunit is mainly on the non-raft fraction, while the β-subunit is distributed on both lipid raft and non-raft fractions.[3] This result prompted us to compare the membrane distribution of α- and β-subunits of WT GPR56 as well as the R565W and L640R mutants, two BFPP mutations in the extracellular loop of β-subunit. As shown in Fig. 7, the WT α-subunit is indeed localized restrictedly at the non-raft fractions and the β-subunit is evenly distributed on the lipid raft and non-raft fractions. The distribution of a GPS cleavage-deficient mutant (GPR56-T383A) is similar to that of the WT β-subunit, confirming the raft-associated localization (supplemental Fig. S7*A*). Most interestingly, although the α-subunits of R565W and L640R mutants are similarly located in the non-raft fractions, their β-subunits are heavily aggregated and localized mostly in the non-raft fractions with only minimum distribution to lipid rafts (Fig. 7*B* and supplemental Fig. S7*B*). These data suggest that the R565W and L640R mutations most likely induce conformational alteration of the 7TM-subunit, leading to the formation of aggregates and the differential distribution on the membrane subdomains.

DISCUSSION

Our extensive analysis of the WT-GPR56 and BFPP-associated point mutants has revealed important biochemical and molecular characteristics of GPR56 receptor that might provide a satisfactory explanation as to how different point muta-

[3] Y.-S. Huang, N.-Y. Chiang, C.-C. Hsiao, H.-Y. Chen, G.-W. Chang, and H.-H. Lin, unpublished results.

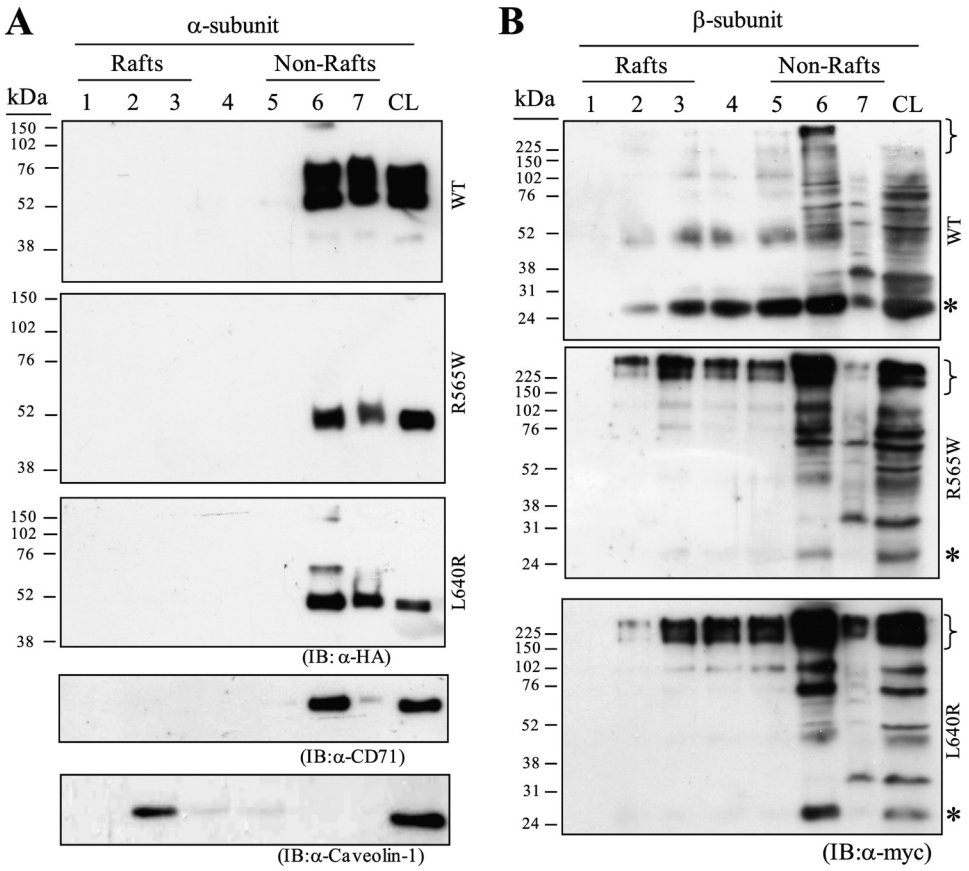

FIGURE 7. **Differential distribution of receptor subunits of GPR56-WT, -R565W, and -L640R mutants in membrane microdomains.** Western blot analysis of the lipid raft fractionation of CHO-K1 cells transfected with GPR56-WT, -R565W, and -L640R using anti-HA (*A*) and anti-Myc (*B*) to detect the α-subunit and β-subunit of GPR56, respectively. The *asterisk* and *curly bracket* denote β-subunit monomer and aggregate, respectively. Caveolin-1 and CD71 were used as positive control proteins for raft- and non raft-fractions, respectively. *CL* stands for cell lysate.

tions cause the same null phenotype. As reported previously and confirmed herein, the major defect caused by the BFPP-associated missense mutations is the defective protein trafficking and reduced membrane expression of GPR56 (19, 26). This result indicates that the functional maturation of GPR56 receptor is highly stringent and depends on its overall conformational stability. Thus, we can conclude the different BFPP-associated point mutations represent amino acid residues important for the proper folding, correct conformation, and hence efficient expression of GPR56. However, the null phenotype observed in BFPP patients cannot be accounted for entirely by the inefficient expression of the GPR56 receptor. Our results suggest that the mutant residues are also involved in different functional aspects of GPR56.

We first showed that GPR56 receptor modification is multifaceted, including extensive glycosylation and proteolytic cleavage (Figs. 1 and 2). As with other adhesion-GPCRs, decoration of GPR56 by glycans is expected due to its 7 potential *N*-glycosylation and numerous *O*-glycosylation residues. Glycosylation is likely an important post-translational modification for the stability, maturation, and function of all adhesion-GPCRs (22). Our data suggest that GPR56 receptor might undergo two independent proteolytic modifications: one by GPS auto-proteolysis and the other by unspecified protease(s). First, mutation engineered to abolish GPS proteolysis did not prevent receptor shedding (Fig. 2, *D* and *E*). Second, deficiency of receptor proteolysis observed in both C346S and W349S disease mutants is consistent with the fact that the two residues are highly conserved in the GPS motif and confirms that they are important for GPS auto-proteolysis (16, 17). Third, shedding of the α-subunit can be greatly inhibited by GM6001, a broad-spectrum MMP/ADAM inhibitor. Our results suggest that the shedding of GPR56 α-subunit is independent of its GPS proteolytic modification. Therefore, GPR56 is expressed either as a two-subunit complex on the cell surface or as a soluble α-subunit and a truncated 7TM receptor.

Although all BFPP-associated mutations reduce the surface expression of GPR56 to some extent, some mutations such as L640R actually retain a high level of surface expression (Figs 1 and 2). This reinforces the idea that apart from reduced surface expression there are probably other mechanisms responsible for the null phenotype of BFPP. Indeed, the identification of a TG2-independent ligand seems to provide one reasonable explanation. The use of GPR56-mFc probe allows a sensitive and efficient means for the identification of GPR56-ligand-expressing cells. Furthermore, it enables us to confirm unambiguously that human TG2 is not a cellular ligand for GPR56. This result not only points to the presence of a novel protein ligand for GPR56 but also challenges the biological relevance of the interaction between human GPR56 and mouse TG2 (20, 27).

Importantly, the failure of the N-terminal mutants (R38W, Y88C, and C91S) to bind to the putative ligand strongly sug-

gests that this protein ligand is relevant to BFPP. Recently, Li *et al.* have also demonstrated the presence of a novel ligand of GPR56 in the ECM of fetal mouse brain using a similar mouse GPR56-mFc protein (11). Their follow-up study further indicated that GPR56 plays a role in maintaining the integrity of pial BM by regulating cell adhesion of developing neurons to the BM molecules (10). Most importantly, it seems that the phenotype induced by the loss of GPR56 is not entirely cell-autonomous. Instead, it is likely that GPR56 binding to the novel ligand might exert a reciprocal signaling via the ligand, leading to the phenotypic changes of ligand-expressing cells. In this context, our finding that GPR56-ligand interaction promotes cell adhesion of ligand-expressing cells fits well with this hypothesis. It will be of great interest in the future to reveal and compare the molecular identity of the novel protein ligand identified here and the ECM ligand reported by Li *et al.* (11).

The differential distribution of the α- and β-subunits of WT GPR56 to the different membrane subdomains (lipid raft and non-raft regions) suggests that the two subunits are not always tightly associated on the plasma membrane. Indeed, treatment of receptor-expressing cells with a weak detergent perfluorooctanoic acid (PFO) shows that GPR56 α- and β-subunits can be differentially dissociated from cell membrane by PFO (supplemental Fig. S7*C*). This result is consistent with earlier data on latrophilin and points to a more complex relationship between the adhesion-GPCR subunits than previously thought (28, 29). As lipid rafts are an important platform for initiating intracellular signaling, it is possible that the localization of the β-subunit to the raft region plays a role in the signaling function of GPR56. Given the relatively normal surface expression of the α-subunit of R565W and L640R mutants, the tendency of their β-subunit to form large aggregate and locate preferentially in the non-raft regions suggest these two TM mutations most likely inactivate GPR56 function by interfering with intracellular signaling and/or the stability of β-subunit.

In conclusion, through the analysis of WT and disease-associated GPR56 mutants we have identified multiple molecular mechanisms relevant to GPR56 biology. These include subcellular trafficking, and expression, GPS auto-proteolysis, receptor shedding, interaction with a novel cellular ligand and differential membrane distribution of receptor subunits. We suggest different BFPP-associated mutations cause the null phenotype via different combination of GPR56 mutant-specific molecular mechanisms.

Acknowledgment—We thank Dr. Martin Stacey for his critical comments.

REFERENCES

1. Bockaert, J., Perroy, J., Bécamel, C., Marin, P., and Fagni, L. (2010) *Annu. Rev. Pharmacol. Toxicol.* **50,** 89–109
2. Daaka, Y. (2004) *Sci. STKE* **2004,** re2
3. Druey, K. M. (2009) *Immunol. Res.* **43,** 62–76
4. Lattin, J., Zidar, D. A., Schroder, K., Kellie, S., Hume, D. A., and Sweet, M. J. (2007) *J. Leukoc. Biol.* **82,** 16–32
5. Spiegel, A. M., and Weinstein, L. S. (2004) *Annu. Rev. Med.* **55,** 27–39
6. Liu, M., Parker, R. M., Darby, K., Eyre, H. J., Copeland, N. G., Crawford, J., Gilbert, D. J., Sutherland, G. R., Jenkins, N. A., and Herzog, H. (1999) *Genomics* **55,** 296–305
7. Zendman, A. J., Cornelissen, I. M., Weidle, U. H., Ruiter, D. J., and van Muijen, G. N. (1999) *FEBS Lett.* **446,** 292–298
8. Shashidhar, S., Lorente, G., Nagavarapu, U., Nelson, A., Kuo, J., Cummins, J., Nikolich, K., Urfer, R., and Foehr, E. D. (2005) *Oncogene* **24,** 1673–1682
9. Della Chiesa, M., Falco, M., Parolini, S., Bellora, F., Petretto, A., Romeo, E., Balsamo, M., Gambarotti, M., Scordamaglia, F., Tabellini, G., Facchetti, F., Vermi, W., Bottino, C., Moretta, A., and Vitale, M. (2010) *Int. Immunol.* **22,** 91–100
10. Koirala, S., Jin, Z., Piao, X., and Corfas, G. (2009) *J. Neurosci.* **29,** 7439–7449
11. Li, S., Jin, Z., Koirala, S., Bu, L., Xu, L., Hynes, R. O., Walsh, C. A., Corfas, G., and Piao, X. (2008) *J. Neurosci.* **28,** 5817–5826
12. Piao, X., Hill, R. S., Bodell, A., Chang, B. S., Basel-Vanagaite, L., Straussberg, R., Dobyns, W. B., Qasrawi, B., Winter, R. M., Innes, A. M., Voit, T., Ross, M. E., Michaud, J. L., Déscarie, J. C., Barkovich, A. J., and Walsh, C. A. (2004) *Science* **303,** 2033–2036
13. Borgatti, R., Marelli, S., Bernardini, L., Novelli, A., Cavallini, A., Tonelli, A., Bassi, M. T., and Dallapiccola, B. (2009) *Clin Genet.* **76,** 573–576
14. Piao, X., Chang, B. S., Bodell, A., Woods, K., Benzeev, B., Topcu, M., Guerrini, R., Goldberg-Stern, H., Sztriha, L., Dobyns, W. B., Barkovich, A. J., and Walsh, C. A. (2005) *Ann. Neurol.* **58,** 680–687
15. Stacey, M., Lin, H. H., Gordon, S., and McKnight, A. J. (2000) *Trends Biochem. Sci.* **25,** 284–289
16. Yona, S., Lin, H. H., Siu, W. O., Gordon, S., and Stacey, M. (2008) *Trends Biochem. Sci.* **33,** 491–500
17. Lin, H. H., Chang, G. W., Davies, J. Q., Stacey, M., Harris, J., and Gordon, S. (2004) *J. Biol. Chem.* **279,** 31823–31832
18. Krasnoperov, V., Lu, Y., Buryanovsky, L., Neubert, T. A., Ichtchenko, K., and Petrenko, A. G. (2002) *J. Biol. Chem.* **277,** 46518–46526
19. Jin, Z., Tietjen, I., Bu, L., Liu-Yesucevitz, L., Gaur, S. K., Walsh, C. A., and Piao, X. (2007) *Hum. Mol. Genet.* **16,** 1972–1985
20. Xu, L., Begum, S., Hearn, J. D., and Hynes, R. O. (2006) *Proc. Natl. Acad. Sci. U.S.A.* **103,** 9023–9028
21. Iguchi, T., Sakata, K., Yoshizaki, K., Tago, K., Mizuno, N., and Itoh, H. (2008) *J. Biol. Chem.* **283,** 14469–14478
22. Hsiao, C. C., Cheng, K. F., Chen, H. Y., Chou, Y. H., Stacey, M., Chang, G. W., and Lin, H. H. (2009) *FEBS Lett.* **583,** 3285–3290
23. Davies, J. Q., Chang, G. W., Yona, S., Gordon, S., Stacey, M., and Lin, H. H. (2007) *J. Biol. Chem.* **282,** 27343–27353
24. Lin, H. H., Stacey, M., Chang, G. W., Davies, J. Q., and Gordon, S. (2005) *BioTechniques* **38,** 696–698
25. Stacey, M., Chang, G. W., Davies, J. Q., Kwakkenbos, M. J., Sanderson, R. D., Hamann, J., Gordon, S., and Lin, H. H. (2003) *Blood* **102,** 2916–2924
26. Ke, N., Ma, H., Diedrich, G., Chionis, J., Liu, G., Yu, D. H., Wong-Staal, F., and Li, Q. X. (2008) *Biochem. Biophys. Res. Commun.* **366,** 314–320
27. Xu, L., and Hynes, R. O. (2007) *Cell Cycle* **6,** 160–165
28. Silva, J. P., Lelianova, V., Hopkins, C., Volynski, K. E., and Ushkaryov, Y. (2009) *The J. Biol. Chem.* **284,** 6495–6506
29. Volynski, K. E., Silva, J. P., Lelianova, V. G., Atiqur Rahman, M., Hopkins, C., and Ushkaryov, Y. A. (2004) *EMBO J.* **23,** 4423–4433